Energy & Buildings 357 (2026) 117112

Contents lists available at ScienceDirect

Energy & Buildings

journal homepage: www.elsevier.com/locate/enbuild

Reduction of heating energy demand by combining IR heaters and IR reflective walls: An experimental study

Lukas Anselm Wille [a,b,*], Björn Schiricke [a], Kai Gehrke [c], Tobias Dehne [d], Bernhard Hoffschmidt [a,b]

[a] Institute of Solar Research, German Aerospace Center (DLR), Linder Höhe, Cologne, 51147, Germany
[b] Chair of Solar Components, RWTH Aachen University, Aachen, 52062, Germany
[c] Institute of Networked Energy Systems, German Aerospace Center (DLR), Carl-von-Ossietzky-Straße 15, Oldenburg, 26129, Germany
[d] Institute of Aerodynamics and Flow Technology, German Aerospace Center (DLR), Bunsenstraße 10, Göttingen, 37073, Germany

ARTICLE INFO

Keywords:
Thermal comfort
IR Heater
PMV
Climate test chamber
Low-ϵ surface

ABSTRACT

In this study, we build upon previous simulation research that advocates the use of infrared (IR) heaters in conjunction with IR reflective interior walls to meet heating demand in buildings. This combination allows the walls to reflect the heat emitted by the IR heaters back to the occupants in a room, rather than absorbing the radiation. As a result, the radiant temperature increases and the air temperature can be lowered in order to maintain constant thermal comfort and to reduce heat loss through the building envelope. We conducted experiments in a climate chamber to isolate the effects of four factors on thermal comfort: the heating power of IR heaters, the IR emittance of the interior walls, the interior wall surface temperature, and the air temperature. The emittance was modified by applying an increasing number of adhesive aluminium foil stripes. Heat conduction through the wall to the outside is not part of this study. To minimize the number of required experiments, we employed a Central Composite Design, from which we derived a response surface function. The experimental results confirm a correlation between wall emittance and occupant thermal comfort in a room, particularly at higher IR heater power levels. The Predicted Mean Vote (PMV) value increases at lower wall emittance (corresponding to higher radiant temperatures), highlighting the potential for energy savings through reduced air temperatures. However, the observed impact of low emittance surfaces on the PMV is less pronounced than previously estimated in simulation studies.

1. Introduction

Energy consumption for heating in buildings is an important factor when trying to reduce carbon emissions in the building sector. This experimental study contributes to the overall goal of efficient and carbon free heating technologies.

1.1. Motivation

Thermal radiation plays a crucial role in thermal comfort of occupants in a building. Along with convective heat transfer and metabolic heat production, it significantly contributes to the thermal balance around occupants in indoor environments. The key principle of this work is to reduce radiation heat loss of occupants by increasing the radiant temperature in the room, allowing for greater convective heat loss to be tolerated. As a result, the air temperature can be lowered, leading to reduced transmission heat loss through the walls and consequently lower heating energy demand. The radiant temperature can be increased using an infrared (IR) heater, which emits a large amount of thermal radiation, in combination with IR reflective wall coatings that reflect the thermal radiation back into the room instead of absorbing it. Several publications exist to assess the energy-saving potential of reflective interior walls in buildings [1–4]. These studies show significant energy saving potential, but only have sparse or no experimental validation. In this work we attempt to close this gap and perform experiments building upon our previous simulations [3].

1.2. Research and typical applications

The importance of thermal radiation and surface emittance in building physics has long been in the focus of scientific work as well as product development. In an early publication, Gläser examined the insulation performance of different reflective coatings in double glazed windows [5]. Since then, double and triple glazed windows have further improved and do not only satisfy thermal comfort needs but also visual comfort demands with different transmittance for visual light [6,7]. But also in

* Corresponding author.
E-mail address: lukas.wille@dlr.de (L.A. Wille).

https://doi.org/10.1016/j.enbuild.2026.117112
Received 8 September 2025; Received in revised form 14 January 2026; Accepted 3 February 2026
Available online 5 February 2026

other parts of the building, optical properties are important aspects that need to be considered. In warmer climates, for example, the sunlight emittance of the outer surface of the building envelope, especially of the roof, plays a key role in the formation of heat islands. Reflective and thermochromic surface materials on the roofs can help to reduce cooling loads in these areas [4,8,9]. In a similar approach, a simulation study with electrochromic materials for an interior wall coating was conducted, where in a winter scenario the IR emittance of the wall was set to a low value (high reflectance) so that radiant heat of an occupant in the room was reflected back to the occupant instead of being absorbed by the cold surrounding walls. This opens the potential to reduce air temperature and save heating energy [1]. In three identical experimental test cabins, Joudi et al. found that application of reflecting wall coatings on the inside as well as the outside can reduce heat exchange with the environment and reduce heating energy demand in winter as well as cooling energy demand in summer [4]. The latter is in contrast to Xu and Raman's simulations [1] who found an energy penalty for reflective interior surfaces in summer. However, in the simulations they do not consider mitigated heat transfer through the walls due to its optical properties.

In the last few decades prices for fossil fuels have risen [10,11], especially since the war in Ukraine caused a rapid increase in gas prices [12], which is why more attention was drawn to electric heating, particularly to IR heaters. They offer a cheap and easy to install alternative to conventional heating systems and require little to no maintenance work. To compensate high operation costs (electric energy) of IR heaters, Heider *et al.* use large PV panels in his field study where they monitor operation and investment costs as well as user satisfaction in a multi-family house [13]. Their results support this setup and see IR heaters as reasonable competition to heat pumps when combined with PV panels. In another field study, Kosack outlines the benefits of higher radiation temperatures and dryer walls caused by the radiation of IR heaters. He compares the heating energy demand of two similar flats where the one, retro-fitted with IR heaters, has a lower heating energy demand than the other flat with a conventional gas heating [14,15]. Recently, the German industry association for IR heaters IG Infrarot and TU Dresden published an article in which they propose to use IR heaters for peak load coverage only, while operating small heat pumps for base load heating which should cover 30% of peak load. The increase in utilization of the heat pump allows for a more cost efficient operation [16]. Furthermore, IG Infrarot, now in cooperation with Fraunhofer IBP, published a comparison of two identical houses, one equipped with a conventional gas heating, the other with IR heaters. They found that the final energy use was nearly identical when maintaining identical thermal comfort. Still, the end energy consumption (total energy delivered to the house) of the IR heaters was 32% less than of the gas heating. This was caused by distribution and combustion losses in the gas heating system. In Stark *et al.*'s recent report from 2024, they look at ways to optimise the use of IR heaters by using them in office buildings with intermittent occupancy and at stationary workplaces. Here, IR heaters have big advantages because they have swift heat up times and can produce good thermal comfort for localized areas. They also compare different radiation and convection heatings and state that there is a need for investigating the influence of surfaces with different emittances [17]. The main indicator that we consider for thermal comfort in this study is the Predicted Mean Vote (PMV, indicator for thermal comfort by Ole Fanger [18], standardized in [19]). The PMV mainly depends on air and radiation temperature, metabolic heat production and the clothing of an occupant in the room.

1.3. Structure of the paper

In the methods part of this paper we describe and explain the experimental setup in the climate test chamber. In the results section we display the results of the experiments and show the limitations of the measurement equipment as well as experimental uncertainties. From the experimental results we derive a response surface function. Finally, we compare the experimental results with those from our previous simulations and identify possible explanations for the differences.

2. Methods

2.1. Geometry and general setup of the experiment

Experiments were performed at the Institute for Energy and Transport, University of Applied Sciences, Zwickau, which operates the climate test chamber the experiments took place in.

The size of the climate test chamber is: 4 m × 4 m × 2.35 m (length × width × height), see Fig. 1. The edge length of the air inlet (Fig. 2a) in the center of the ceiling is 45 cm × 45 cm (length × width). The grille directs the airflow towards the four corners of the room at floor level. To achieve a uniform inlet air velocity, we used a perforated metal plate as well as two layers of a non-woven fabric in the ventilation box above the grille. Test measurements with a handheld anemometer showed uniform velocity distribution across the four inlet directions of the grille. For the outlet we left a gap in the door to the climate chamber, as the walls in the chamber could not be modified and the position of the outlet plays a minor role for the flow distribution in a room [20].

We used two "ETHERMA LAVA-BASIC-325EP" IR heaters with an edge length of 593 mm × 593 mm (height × width) and a maximum power output of 325 W at 230 V each. The two IR heaters were mounted centrally on opposite walls. Due to the depth of the IR heater and the stand, the IR heater surface was 5 cm in front of the wall. The gap between the backside of the heater and the wall was filled with insulating foam to prevent convection heat transfer on the backside.

The wall surface temperature could be adjusted to the desired value using capillary tube mats installed behind the wall cladding. In order to include the ventilation pipe in the ceiling, a separate drywall ceiling was installed using capillary tube mats from "Clina" (see Fig. 2b). The tube mats did not cover the entire ceiling area, which is why we worked with an area-weighted mean temperature T_{mean} from the "active" ceiling area (temperature controlled/with tube mats behind) and the passive area (with no tube mats behind). Similarly to the ceiling, the door to the climate chamber did not have active temperature control which is why we took the area weighted mean temperature of the active wall and the passive door. The active area of the ceiling is $f_{\mathrm{active,ceiling}} = 0.7$ of the total ceiling area. The active area of the one wall, in which the passive door is, is $f_{\mathrm{active,wall}} = 0.8$. All other walls, including the floor, are entirely temperature controlled. Mean temperature is calculated using:

$$T_{\mathrm{mean}} = f_{\mathrm{active}} T_{\mathrm{active}} + (1 - f_{\mathrm{active}}) T_{\mathrm{passive}} \tag{1}$$

In order to achieve the required emittance of the surface, we used a similar approach. We combined two different surface materials, one with high emittance and one with low emittance. Together they form the desired average/cumulative emittance (Fig. 3). The high emitting surface is an orange polymer adhesive film usually used for car wrapping. The low emitting surface is adhesive aluminium foil. The emittance was measured between 2.5–16 µm using an IR spectrometer at the OPAC laboratory (Almería, Spain), which is a collaboration between DLR and CIEMAT, the Spanish owner of the Plataforma Solar de Almería. For more information see Appendix A.1. The measured values are: orange adhesive film $\epsilon_{\mathrm{high}} = 0.94$, aluminium foil $\epsilon_{\mathrm{low}} = 0.031$. The materials are opaque. To acquire different values for the interior surface emittance, each surface is divided into 0.5 m wide segments. Each segment is split into four sub-segments. The sub-segments are 88 mm + 162 mm + 162 mm + 88 mm = 500 mm wide. Stripes of the aluminium foil with according width are then stuck onto the orange film as illustrated in Fig. 3 forming different average emittances for each segment. This way, five different values for the emittance of the whole surface can be achieved: 1. no stripes, 2. one stripe, 3. two stripes, 4.

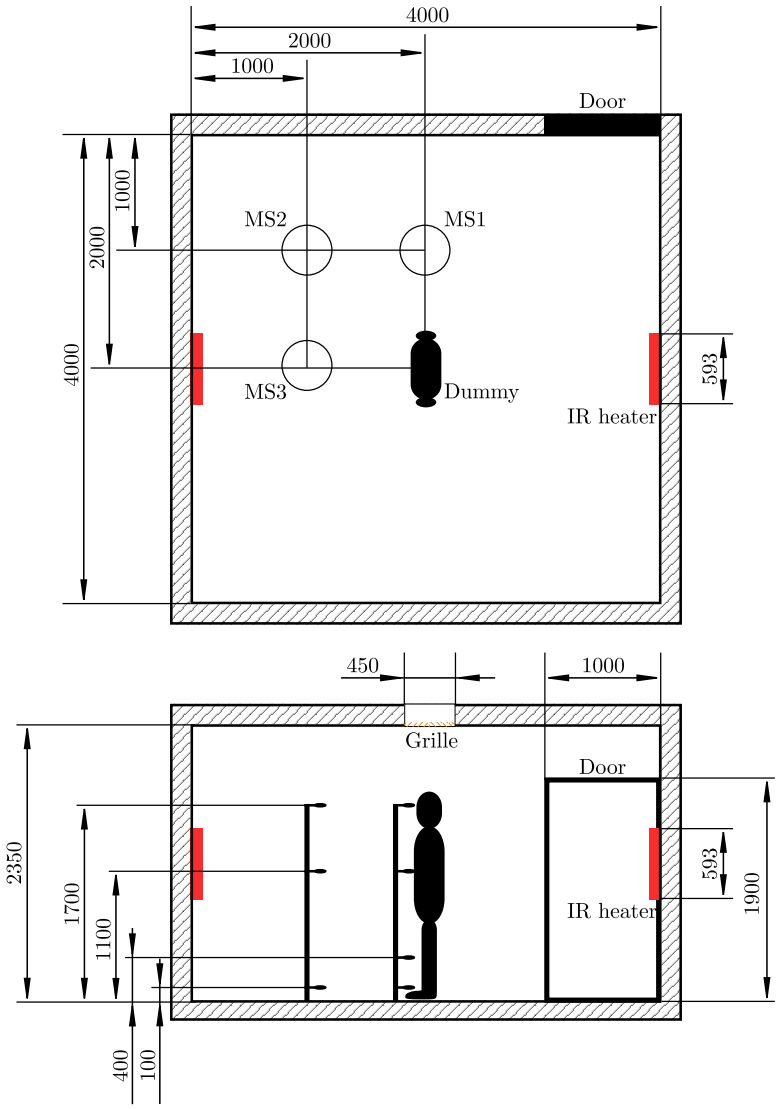

Fig. 1. Climate test chamber with the two IR heaters, the measurement stands MS1, MS2, MS3 and the dummy. Dimensions in mm.

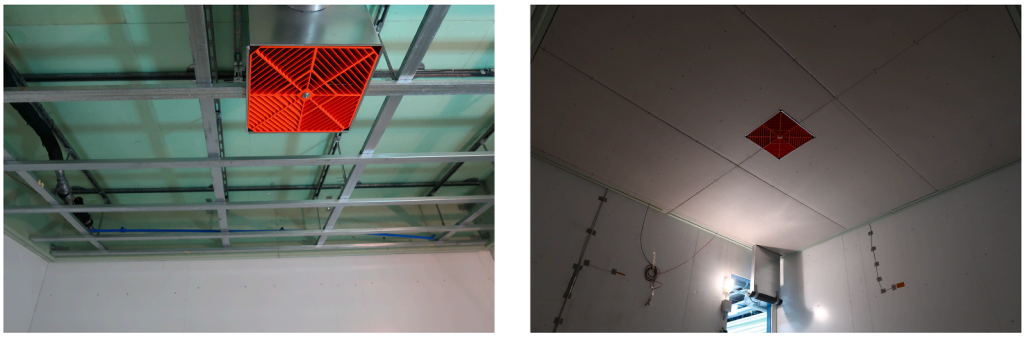

(a) Orange air inlet grille with the ventilation box before the heated Clina ceiling was put in.

(b) Final ceiling setup with the grille, the heated Clina ceiling and the air pipe at the door.

Fig. 2. Ceiling setup in the climate chamber.

three stripes, 5. fully covered. The mean emittance ϵ is calculated using:

$$\epsilon = \frac{A_{\text{low}}\epsilon_{\text{low}} + A_{\text{high}}\epsilon_{\text{high}}}{A_{\text{low}} + A_{\text{high}}} \tag{2}$$

The dummy representing an occupant in the climate chamber has a surface area of $1.52\,\text{m}^2$, a metabolic heat generation of $80\,\text{W/m}^2$ ($1.38\,\text{met}$) which sums up to a total power output of $P_{\text{dummy}} = 122\,\text{W}$. The surface emittance is $\epsilon_{\text{dummy}} = 0.92$. The dummy is placed in the middle of the room, between the IR heaters.

To determine the thermal comfort value PMV of the dummy, we used a “ComfortSense Dantec Dynamics” measuring setup with one hygrometer, one sensor for the operative temperature and eight anemometers,

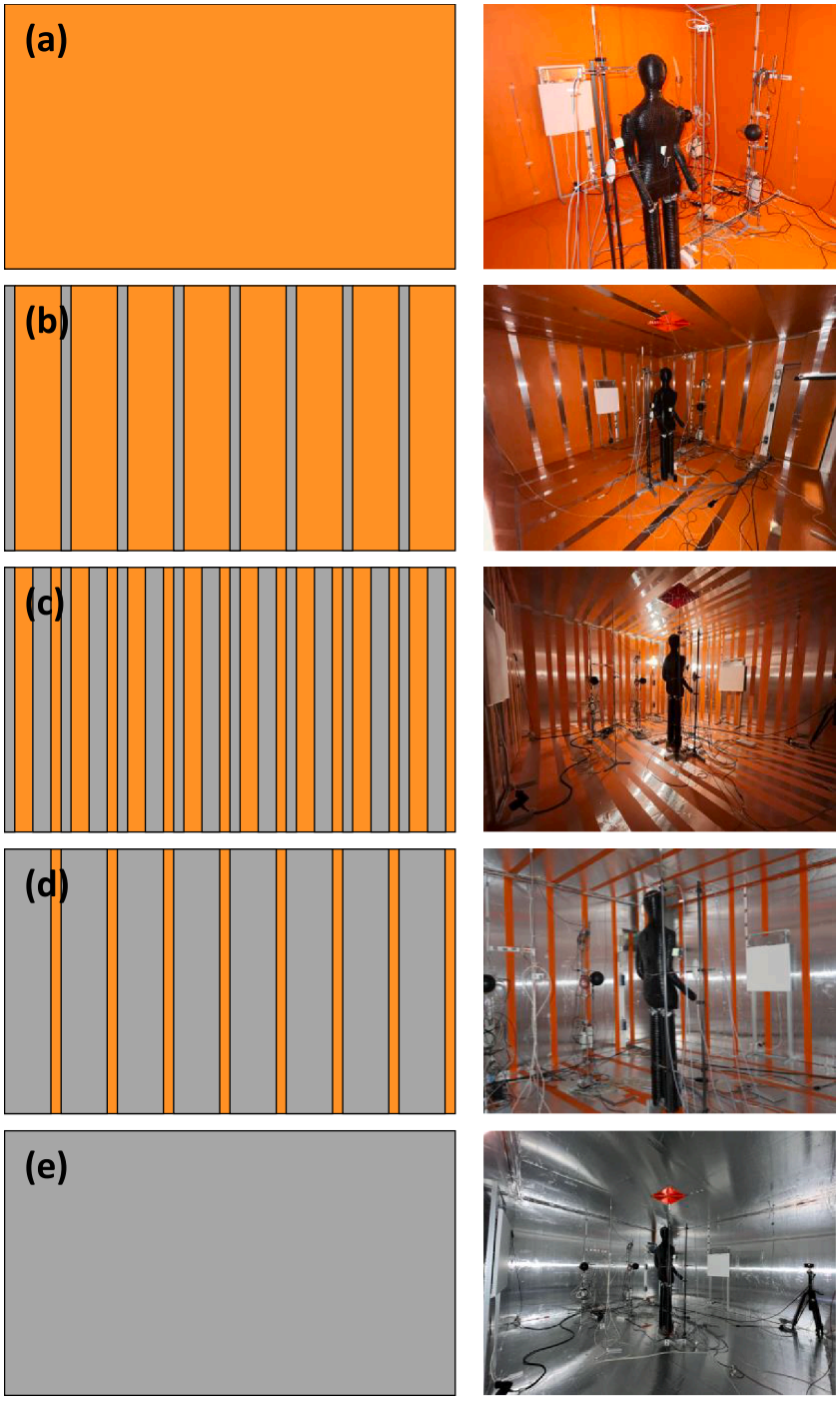

Fig. 3. Five different stages of emittance of the walls with averaged values from high to low: **a**: $\epsilon = 0.94$, **b**: $\epsilon = 0.78$, **c**: $\epsilon = 0.49$, **d**: $\epsilon = 0.19$, **e**: $\epsilon = 0.03$.

each anemometer combined with a thermometer. According to DIN EN ISO 7726 for standing people, measuring heights were at 0.1 m, 1.1 m and 1.7 m. Additionally we measured at 0.4 m .The data logger was placed outside the climate chamber to reduce thermal loads within.

Additionally to the Dantec system at the dummy, there were three more measurement stands in the room. The location of the stands can be seen in Fig. 1. The exact placement of the sensors is as follows:

- Dummy and Dantec system in middle of the room, facing the IR heater
  - 0.1 m over ground: one combined anemometer and thermometer 5 cm in front of the dummy and one 5 cm next to the dummy
  - 0.4 m over ground: one combined anemometer and thermometer 5 cm in front of the dummy and one 5 cm next to the dummy
  - 1.1 m over ground: one combined anemometer and thermometer 5 cm in front of the dummy and one 5 cm next to the dummy. Additional sensor for operative temperature next to the dummy (35 cm from the center of the room)
  - 1.7 m over ground: one combined anemometer and thermometer 5 cm in front of the dummy and one 5 cm next to the dummy
  - 2 m over ground: hygrometer (25 cm × 25 cm from the center of the room)
- measuring stand MS1, centered between the IR heaters, 1 m from the side wall

  - 0.1 m over ground: thermometer
  - 1.1 m over ground: thermometer, globe thermometer, anemometer, hygrometer
  - 1.7 m over ground: thermometer
- measuring stand MS2, in the corner, 1 m from both walls
  - 0.1 m over ground: thermometer
  - 1.1 m over ground: thermometer, globe thermometer, anemometer (for single measurement only)
  - 1.7 m over ground: thermometer
- measuring stand MS3, centered, 1 m from IR heater
  - 0.1 m over ground: thermometer
  - 1.1 m over ground: thermometer
  - 1.7 m over ground: thermometer

The temperature of the surfaces in the climate chamber was measured and controlled using Pt100 sensors glued to the surface. Each of the surfaces had its own temperature control to ensure accurate temperatures.

The central air conditioning system of the lab building supplied the preconditioned air volume flow for the air inlet into the climate chamber. The air was then heated to the required set point using an electric heater in the supply pipe. The volume flow was measured by a "HESCO V-CONTROL CRNS DN160". A differential pressure is generated in the measuring orifice by a flow restriction body with a defined pressure loss characteristic curve, which is detected by a pressure transmitter and converted into a flow rate. To measure the temperature of the volume flow, nine temperature sensors were fitted inside the pipe. The volume flow was set to 500 m^3h^{-1}, which corresponds to 13.3 air changes per hour. This high rate was chosen in order to decouple the air temperature in the chamber from the wall temperature. Humidity in the inlet air flow was not controlled but resulted from outside weather conditions and was measured by the two hygrometers in the room.

2.2. Design of experiments

For the design of the experimental plan, we used a Central Composite Design, because it can capture both the quadratic effects of the parameters as well as the interactions between the different parameters and their impact on the PMV [21]. A Central Composite Design is a response surface methodology that forms a n-dimensional cube in the factor space with axial star points and center points, enabling efficient estimation of quadratic effects and interactions. The experimental parameters follow the same Central Composite Design as those in our previous simulation study [3]. However, the experimental plan had to be adjusted as the emittance of the real surface materials differed from the parameters originally set in the simulations. Also the IR heaters did not reach their maximum power output of 325 W which is why two star points with minimum and maximum power output were moved closer together than in the standard Central Composite Design (star points No. 17 and No. 18). Table 1 shows the input parameters for the experiments: wall temperature T_{wall}, inlet air temperature T_{inlet}, emittance of the interior surfaces ϵ and the IR heater power P_{ir}.

2.3. Differences between experiment and simulation model

Experiments were designed to be as close to our previous simulations [3] as possible. However, there are some differences which we summarize in the following list:

- The dummy is closer to the shape of a human and not a simplified cuboid, the emittance is $\epsilon_{dummy} = 0.92$ instead of $\epsilon_{dummy,simulation} = 0.9$.
- The air outlets are not equally distributed among all four walls but is through a gap at the door to the climate chamber.
- As the heaters did not reach their maximum power output with the voltage of the local electrical grid in Zwickau, the combined maximum power output of the two IR heaters is at 600 W (300 W each heater) instead of 648 W at point No. 18. Therefore, point No. 17 was adjusted accordingly to 120 W.
- The emittance of the walls was combined by stripes of two materials instead of being a homogeneous surface.
- Due to the physical expansion of the baffles in the grille, the ventilation box had to be designed 5 cm larger. The open cross section remains the same size.
- The edge length of the IR heaters was 7 mm smaller than in the simulations.
- The heating panels did not sit flush with the wall surface but protrude by 5 cm due to the mounting brackets and the stand.
- The spread of the wall emittance is between $\epsilon_{high} = 0.94$ and $\epsilon_{low} = 0.031$ instead of $\epsilon_{high,simulation} = 0.9$ and $\epsilon_{low,simulation} = 0.1$.

Table 1
Experimental plan according to a Central Composite Design with four parameters and three center points (CP) and the order in which the experiments were conducted. Parameters are wall temperature T_{wall}, inlet air temperature T_{inlet}, emittance of the interior surfaces ϵ and the IR heater power P_{ir}.

No.	T_{wall} °C	T_{inlet} °C	ϵ -	P_{ir} W	Order -
1	14.2	16.4	0.19	174	25
2	14.2	21.6	0.19	174	21
3	18.8	16.4	0.19	174	23
4	18.8	21.6	0.19	174	19
5	14.2	16.4	0.78	174	8
6	14.2	21.6	0.78	174	4
7	18.8	16.4	0.78	174	6
8	18.8	21.6	0.78	174	2
9	14.2	16.4	0.19	546	26
10	14.2	21.6	0.19	546	22
11	18.8	16.4	0.19	546	24
12	18.8	21.6	0.19	546	20
13	14.2	16.4	0.78	546	9
14	14.2	21.6	0.78	546	5
15	18.8	16.4	0.78	546	7
16	18.8	21.6	0.78	546	3
17	16.5	19	0.49	120	13
18	16.5	19	0.49	600	15
19	16.5	19	0.03	360	27
20	16.5	19	0.94	360	1
21	13	19	0.49	360	16
22	20	19	0.49	360	12
23	16.5	15	0.49	360	17
24	16.5	23	0.49	360	11
25 (CP1)	16.5	19	0.49	360	10
26 (CP2)	16.5	19	0.49	360	14
27 (CP3)	16.5	19	0.49	360	18

3. Results and discussion

3.1. Experiments

The measured data was preprocessed to calculate the PMV using the python package "pythermalcomfort" [22]. The PMV at the dummy was calculated using the PMV from each sensor located at the dummy and averaging it. For each PMV value the air temperature T_{air} and velocity v_{air} of the eight Dantec sensors at the dummy were taken. The mean radiant temperature T_{mrt} was calculated from the Dantec measuring software ComfortSense using the operative temperature sensor as well as the air temperature and velocity next to the dummy at 1.1 m height which was directly next the operative temperature sensor. Information on signal conversion formula can be found on Dantec's website [23]. As the humidity in the test chamber could not be controlled and mainly depended on the outside weather conditions, the PMV was calculated assuming a constant relative humidity of $\phi = 50\%$. This way the results can be compared to each other without the influence of humidity. Clothing factor is fixed to 1 clo, metabolism to 1.38 met for all PMV calculations. These

parameters represent a person doing light sitting and standing work and wearing long trousers and a jumper (see ISO 7730 [19]).

To receive the PMV for measurement stand MS1 and MS2 the mean radiant temperature T_{mrt} was calculated from the globe temperature sensor T_{glo} using Eq. 3:

$$T_{mrt} = \left(\left(T_{glo} + 273.15\right)^4 + \frac{h_{cg}}{h_r} \cdot \left(T_{glo} - T_{air}\right) \right)^{\frac{1}{4}} - 273.15 \quad (3)$$

with

$$h_{cg} = \max\left(\frac{6.3 \cdot v_{air}^{0.6}}{D^{0.4}},\ 1.4 \cdot \left(\frac{|T_{glo} - T_{air}|}{D} \right)^{0.25} \right)$$

where T_{air} and v_{air} are read from sensors at the same position as the globe thermometer. $D = 150\,\text{mm}$ is the diameter of the globe thermometer, and $h_r = \epsilon\sigma$. Emittance of the globe thermometer is $\epsilon = 0.95$, $\sigma = 5.67 \cdot 10^{-8}\,\text{Wm}^{-2}\text{K}^{-4}$ is the Stefan-Boltzmann constant. Again, relative humidity was fixed to 50%. Calculation of T_{mrt} from the operative temperature sensor from Dantec is very similar and shown in Appendix A.3. Limited resources did not allow for an anemometer at MS2 for all measurements. Instead, we swapped the anemometer from MS1 to MS2 for a single extra measurement. This measurement was assumed constant for all other measurements and taken to calculate PMV at MS2. This reduces accuracy at MS2, however, the measured air velocities were low (0.036–0.098 m/s at MS1 and 0.108 m/s at MS2) with small overall impact on the PMV. We then calculated the PMV for each thermometer on MS1 and MS2 and averaged the values into one PMV value for MS1 and one for MS2 respectively.

For each measurement we adjusted all parameter controls of the climate chamber until we reached steady state conditions. Then a 30 minute data acquisition started. The data was then averaged over the interval into one value for each sensor and measurement. If during the measurement one or more parameters diverged from the required set point, we repeated the measurement. Table 2 shows the measured PMVs for each measurement at the dummy, at MS1 and at MS2.

In the results, an increase in PMV is expected for lower interior surface emittance, as more heat is reflected back to the dummy, raising the mean radiant temperature and thus the PMV.

This trend can be observed in the measurements for low-emittance surfaces by examining paired data points in which only one parameter differs. Thanks to the Central Composite Design used in our experimental plan, the cubic structure ensures that for each parameter set, a corresponding set exists where only a single parameter is varied.

When comparing pairs of measurements in which the wall emittance is the only variable while the other three parameters remain constant, a clear increase in PMV is evident for lower wall emittance. For instance, between measurements No.,1 and 5, the PMV rises by 0.06 (from −0.8 to −0.74). Another aspect we can see in the data is that this effect becomes more prominent for higher IR heater power, as there is more radiation to be reflected and therefore, to increase the mean radiant temperature. For No. 9 and 13, the corresponding measurements to No. 1 and 5 with higher heating power, the measured difference in PMV is already at 0.15 (from −0.69 to −0.54). This effect can also be seen for all other pairs, especially at No. 19 and 20, the pair where the emittance changes from 0.94 to 0.03 and the PMV form −0.33 to 0.01.

To express this in possible energy savings, we take PMV = −0.33 from No. 20 at the dummy that was calculated with the values $T_{air} = 18.0$, $T_{mrt} = 18.5$, $v_{air} = 0.1$, $\phi = 50\%$, 1.38 met, 1 clo. While fixing all other values, we then increase the air temperature T_{air} in the PMV calculation by 3.4 °C up to 21.4 °C to match PMV = 0.01 from No. 19. Assuming all other values remain constant, this means that reducing the emittance has the same effect as increasing the air temperature by 3.4 °C. The IR images in Fig. 4 underline how the heat is reflected from the wall when the emittance of the interior surfaces is low. While in Fig. 4 only the warm surfaces of the IR heater and the dummy are visible, the reflection in Fig. 4 can easily be seen and causes a higher radiant temperature. There is no color bar included since the high radiant component as well as multiple reflections and different surface emittances make an exact quantitative evaluation of the IR images impossible.

Table 2
Experimental results including three center points (CPs) with all four parameters (wall temperature T_{wall}, inlet air temperature T_{inlet}, emittance of the interior surfaces ϵ and the IR heater power P_{ir}). Average air temperature T_{air} of all thermometers in the room and the PMV and the dummy, measuring stand MS1 and MS2.

No.	T_{wall} °C	T_{inlet} °C	ϵ -	P_{ir} W	T_{air} °C	PMV_{dummy} -	PMV_{MS1} -	PMV_{MS2} -
1	14.1	16.3	**0.19**	174	15.6	**−0.74**	−0.81	−0.83
2	14.1	21.3	0.19	174	17.2	−0.50	−0.58	−0.51
3	18.7	16.2	0.19	174	18.5	−0.17	−0.21	−0.25
4	18.8	21.5	0.19	174	20.4	0.16	0.08	0.05
5	14.2	16.5	**0.78**	174	15.6	**−0.80**	−0.88	−0.89
6	14.1	21.7	0.78	174	17.1	−0.58	−0.68	−0.59
7	18.7	16.3	0.78	174	18.6	−0.18	−0.25	−0.29
8	18.8	21.4	0.78	174	20.2	0.07	−0.02	−0.05
9	14.2	16.4	**0.19**	546	16.2	**−0.54**	−0.63	−0.65
10	14.1	21.6	0.19	546	17.8	−0.29	−0.37	−0.31
11	18.7	16.5	0.19	546	19.2	0.03	−0.01	−0.08
12	18.7	21.4	0.19	547	20.8	0.34	0.27	0.21
13	14.2	16.5	**0.78**	546	15.8	**−0.69**	−0.82	−0.82
14	14.3	21.7	0.78	548	17.5	−0.45	−0.58	−0.47
15	18.8	16.3	0.78	546	18.9	−0.07	−0.16	−0.20
16	18.8	21.8	0.78	547	20.6	0.20	0.07	0.05
17	16.5	19.0	0.49	120	17.8	−0.37	−0.45	−0.47
18	16.5	19.0	0.49	600	18.3	−0.19	−0.30	−0.32
19	16.4	19.0	**0.03**	360	18.8	**0.01**	−0.03	−0.11
20	16.4	19.0	**0.94**	360	18.0	**−0.33**	−0.44	−0.45
21	13.0	19.1	0.49	360	15.8	−0.77	−0.86	−0.78
22	20.0	18.9	0.49	360	20.4	0.17	0.12	0.07
23	16.4	15.0	0.49	360	16.8	−0.51	−0.56	−0.59
24	16.5	23.1	0.49	360	19.3	−0.12	−0.20	−0.15
25	16.4	19.1	0.49	360	18.1	−0.29	−0.38	−0.40
26	16.4	18.9	0.49	360	18.0	−0.30	−0.39	−0.41
27	16.5	19.1	0.49	360	18.1	−0.29	−0.38	−0.40

To evaluate the experimental precision, we performed three repeated measurements at the center point (No. 25, 26 and 27) with the same parameter settings. The measured PMV values are −0.295, −0.301, and −0.287. The calculated mean is −0.294 with a standard deviation of 0.006. This low standard deviation indicates a high level of reproducibility and precision of the experimental setup. The observed variability can primarily be attributed to random experimental errors, which are considered negligible in comparison to the magnitude of the measured response. This level of precision ensures the reliability of the data and supports the validity of the derived model.

3.2. Response surface

From the measured PMV of the dummy in Table 2, we derive the function for $PMV = f(T_{wall}, T_{air}, \epsilon, P_{ir})$ using a multiple linear regression approach with codified variables. T_{air} is the mean air temperature of the eight thermometers at the dummy. The p-value was kept below 0.05, all other terms were left out from the final Eq. 4 one by one. This is the non-codified form:

$$\begin{aligned} PMV = &-0.1703 \\ &+ 0.02624(T_{wall} - 16.5) \\ &+ 0.1643(T_{air} - 19) \\ &- 0.1572(\epsilon - 0.5) \\ &+ 0.0002108(P_{ir} - 360) \\ &+ 0.4069(\epsilon - 0.5)(\epsilon - 0.5) \\ &- 0.000245(\epsilon - 0.5)(P_{ir} - 360) \end{aligned} \quad (4)$$

The first term is the PMV offset. After that are the four linear terms for the four variables T_{wall}, T_{air}, ϵ and P_{ir}. T_{air} has the biggest linear impact on the PMV over the parameter range considered in the

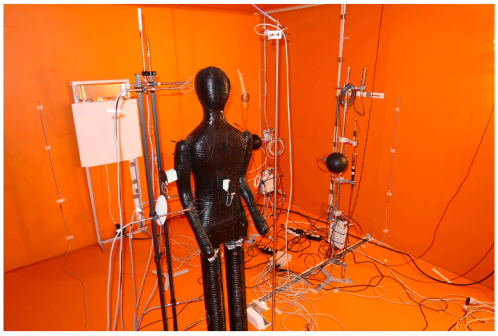

(a) Experimental setup for measurement No. 20 with high emittance surfaces (no aluminum foil).

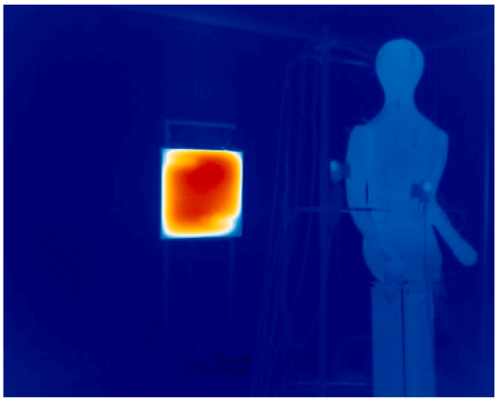

(b) IR image during experiment No. 20.

(c) Experimental setup for measurement No. 19 with low emittance surfaces (surface fully covered with aluminum foil).

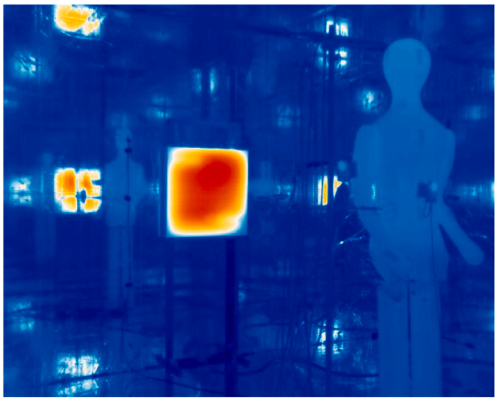

(d) IR image during low-emittance experiment No 19.

Fig. 4. Qualitative comparison of experimental setups and IR images for high and low emittance surfaces. Reflections of IR heater can be seen.

experiments since its (normalized) coefficient is the largest. The negative sign for the linear emittance term underlines the energy saving potential since PMV decreases with higher emittance. The last two terms describe the quadratic behaviour of ϵ and the interaction between ϵ and P_{ir}. This interaction of emittance and IR heater power supports the concept that there is potential energy saving combining the two.

This function can be used to set up a control for IR heaters in an office or a domestic building. While a room is kept at a low temperature during times of no occupation, the IR heater is turned on when someone enters the room. The short warming-up time of the heater quickly increases radiant temperature until satisfying PMV is reached. The control keeps heating power at the right setting according to the response surface function. Here the IR heater makes use of its swift response times and reaches thermal comfort after a short time. A system like this would be particularly useful in uninsulated rooms with short, intermittent occupation. To adapt the control to rooms of different sizes, further development of the technology has to be done.

3.3. Comparison of experiments to simulation

Previous simulations that were the basis for this experimental campaign show great energy saving potential for reflective interior surfaces and IR heaters [3]. The dimensions and the ventilation of the simulations match the geometry of the climate test chamber and apart from small changes the same experimental plan was used. Although, the simulation data suggested a significant influence of heating power and emittance on heating energy demand, the comparison shows that the simulations overrated their influence, mitigating the energy saving potential in the experiments. Fig. 5 shows how much the air temperature set point could be lowered when reducing surface emittance from high to low for simulations of Xu *et al.* [1], our previous simulations [3] and the corresponding experiments presented in this paper. Xu *et al.* found the largest difference in their simulations, even though they did not account for any additional heat sources in the room and only considered body heat of the occupant to increase radiant temperature. In contrast, our simulations and the experiment did include additional heat sources with higher

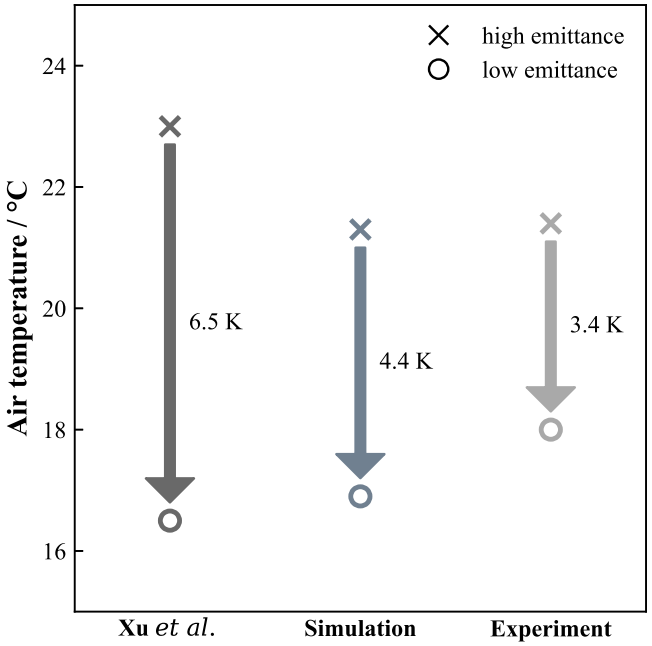

Fig. 5. Possible air temperature reduction when using interior walls with low emittance according to the work of: simulations from Xu *et al.* [1], our previous simulations [3], experiments from this work.

power output, yet resulted in a smaller possible air temperature reduction.

Schmitt and Kriegel [24] give a possible reason in their recent work. They explain that the radiant influence of air can not always be neglected in building simulations. Especially in simulations of large rooms and halls, absorption in air becomes more relevant, since the distance travelled through the air by radiation before being absorbed on a surface (path length) is far. In our test chamber the distance between the IR heater and the dummy is relatively small. However, repeated reflections on the walls result in a considerably longer path length and therefore increased influence of absorption in air.

4. Conclusion

So far, simulation studies have shown great energy saving potential of IR reflective walls with low temperature/convection heatings or no extra heaters at all. Xu *et al.* showed that small heat sources (in form of other occupants) can significantly increase radiant temperature and thermal comfort (PMV) when emittance of the wall is low [1]. This work follows the attempt to maximize this potential of high radiant heat and low emittance. On one side, we increase radiant heat by using heat sources at a higher temperature than normal convection heatings. On the other side, we use adhesive aluminium foil with an emittance lower than 0.1. This way we want to maximize the effect of reflective walls. With both, globe and operative thermometer, we were able to measure an increase of radiant temperature when lowering emittance of the walls. Consequently, we observed higher PMV values. However, the experiments do not show the expected magnitude of this effect. In simulations from Xu *et al.* the temperature set point could be lowered by 6.5 -C with only one occupant inside the room as heat source, with three occupants in the room the set point reduction grows to 8.2 -C. In the experiments we had more extreme values (lower emittance and higher heating power) but still the change in PMV and the therefore possible temperature set point reduction were smaller. Future investigations have to improve ways of simulating and measuring thermal comfort when radiant heat plays a major role, which may include the influence of IR absorbance in air. This way the benefit IR reflective surfaces of interior walls on the energy performance can be used precisely to further mitigate energy consumption and CO_2 emissions.

CRediT authorship contribution statement

Lukas Anselm Wille: Writing – original draft, Visualization, Methodology, Investigation, Formal analysis, Conceptualization; **Björn Schiricke:** Writing – review & editing,Supervision,Methodology,Conceptualization; **Kai Gehrke:** Writing – review & editing, Supervision, Methodology, Conceptualization; **Tobias Dehne:** Writing – review & editing, Supervision, Methodology, Conceptualization; **Bernhard Hoffschmidt:** Writing – review & editing, Supervision, Conceptualization.

Data availability

Data will be made available on request.

Funding

This research received funding from DLR Institute of Solar Research.

Declaration of interests

Lukas Wille reports equipment (two IR heaters) was provided by ETHERMA. If there are other authors, they declare that they have no known competing financial interests or personal relationships that could have appeared to influence the work reported in this paper.

Disclosure statement

The authors report there are no competing interests to declare. Text creation was aided by AI tools. The authors checked the text and take responsibility for the content.

Acknowledgments

Etherma supported this research by supplying the two IR heaters used in the experiments. The Institute for Energy and Transport, University of Applied Sciences in Zwickau conducted the experimental campaign and received payment from the Institute of Solar Research, German Aerospace Center.

Appendix A

A.1. Emittance measurements

The emittance of the aluminium foil, the orange adhesive film and the IR heater was measured with a Perkin Elmer Lambda 1050 on the spectral range 0.28–20 µm. This bandwidth was chosen because the energy maximum for relevant temperatures of 20–100-C lies here. However, above and below that bandwidth there is energy not considered in this study. The emittance is a function of the wavelength, therefore, the values had to be integrated and weighted over the characteristic Planck spectrum. Results are shown in Table A.1.

Table A.1
Emittance ϵ measurement for different radiant temperatures/spectrums.

Surface	20 -C	50 -C	100 -C
Aluminium foil	0.0307	0.0309	0.0313
Orange adhesive film	0.9418	0.9350	0.9207
IR heater	0.9331	0.9323	0.9290

Table A.2
Dantec sensors used during experiments and their accuracy for the conditions they were used in.

Sensor	Location	Accuracy
54T33 temperature	Dummy	±0.2 K
54T33 anemometer	Dummy	±2% or ±0.02 m/s
54T37 hygrometer	Dummy	±1.5% RH
54T38 operative temperature	Dummy	±0.2 K

Table A.3
Sensors used for MS1-3 and the operation of the test chamber. (*only for one meausurement).

Sensor	Location	Accuracy
Volume flow	Main air supply	±4.0%
Surface temperatures	All walls	±0.15 K
Globe temperature	MS1, MS2	±0.15 K
Air temperature	MS1, MS2, MS3 and air supply	±0.15 K
Hygrometer	MS1	±3% RH
Anemometer	MS1, MS2*	±0.015 m/s
Electrical power meter	IR heaters	±0.5%

A.2. DoE Base equation and codified equation

$$\begin{aligned}\mathrm{PMV} = {} & \beta_0 \\ & + \beta_1 T_{\mathrm{wall}} + \beta_2 T_{\mathrm{wall}}^2 + \beta_3 T_{\mathrm{air}} + \beta_4 T_{\mathrm{air}}^2 \\ & + \beta_5 \epsilon + \beta_6 \epsilon^2 + \beta_7 P_{\mathrm{ir}} + \beta_8 P_{\mathrm{ir}}^2 \\ & + \beta_9 T_{\mathrm{wall}} T_{\mathrm{inlet}} + \beta_{10} T_{\mathrm{wall}} \epsilon + \beta_{11} T_{\mathrm{wall}} P_{\mathrm{ir}} \\ & + \beta_{12} T_{\mathrm{inlet}} \epsilon + \beta_{13} T_{\mathrm{inlet}} P_{\mathrm{ir}} + \beta_{14} \epsilon P_{\mathrm{ir}}\end{aligned} \tag{A.1}$$

$$\begin{aligned}\mathrm{PMV} = {} & -0.1703 \\ & + 0.05937\, T_{\mathrm{wall}} + 0.4249\, T_{\mathrm{air}} \\ & - 0.04064\, \epsilon + 0.03925\, P_{\mathrm{ir}} \\ & + 0.02721\, \epsilon^2 - 0.01180\, \epsilon\, P_{\mathrm{ir}}\end{aligned} \tag{A.2}$$

A.3. Sensors

To acquire the mean radiant temperature from the operative temperature sensor from dantec, we used [23], with operative temperature T_{OT}, mean radiant temperature T_{MRT} and air temperature T_{AIR}:(Table A.2 and Table A.3)

$$T_{\mathrm{MRT}} = \sqrt[4]{(T_{\mathrm{OT}} + 273.15)^4 + \frac{h_{\mathrm{c,g}}}{h_{\mathrm{r}}} (T_{\mathrm{OT}} - T_{\mathrm{AIR}})} - 273.15 \tag{A.3}$$

where the radiative heat transfer coefficient h_r can be expressed using the Stefan–Boltzmann constant as

$$h_{\mathrm{r}} = \varepsilon \cdot \sigma = 0.95 \cdot 5.67 \cdot 10^{-8}$$

and the convective heat transfer coefficient $h_{\mathrm{c,g}}$ can be expressed as the maximum value between forced and free convection:

$$h_{\mathrm{c,g}} = \max \begin{cases} 18 \cdot v_{\mathrm{AIR}}^{0.55}, \\ 3 \cdot |T_{\mathrm{OT}} - T_{\mathrm{AIR}}|^{0.25} \end{cases}$$

References

[1] J. Xu, A.P. Raman, Controlling radiative heat flows in interior spaces to improve heating and cooling efficiency, iScience 24 (8) (2021) 102825. https://doi.org/10.1016/j.isci.2021.102825

[2] S. Malz, W. Krenkel, O. Steffens, Infrared reflective wall paint in buildings: energy saving potentials and thermal comfort, Energy Build. 224 (2020) 110212. https://doi.org/10.1016/j.enbuild.2020.110212

[3] L.A. Wille, B. Schiricke, K. Gehrke, B. Hoffschmidt, Reduction of heating energy demand by combining infrared heaters and infrared reflective walls, Buildings 14 (7) (2024). https://doi.org/10.3390/buildings14072183

[4] A. Joudi, H. Svedung, C. Bales, M. Rönnelid, Highly reflective coatings for interior and exterior steel cladding and the energy efficiency of buildings, Appl. Energy 88 (12) (2011) 4655–4666. https://doi.org/10.1016/j.apenergy.2011.06.002

[5] H.J. Gläser, Improved insulating glass with low emissivity coatings based on gold, silver, or copper films embedded in interference layers, Glass Technol. 21 (1980) 254–261.

[6] J. Mohelnikova, H. Altan, Evaluation of optical and thermal properties of window glazing, Wseas Trans. Environ. Dev. 5 (1) (2009) 86–93.

[7] A. Ganji Kheybari, M. Alwalidi, C. Hepf, T. Auer, S. Hoffmann, A multi-objective evaluation for envelope refurbishments with electrochromic glazing, Result. Eng. 14 (2022) 100417. https://doi.org/10.1016/j.rineng.2022.100417

[8] C. Fabiani, A.L. Pisello, E. Bou-Zeid, J. Yang, F. Cotana, Adaptive measures for mitigating urban heat islands: the potential of thermochromic materials to control roofing energy balance, Appl. Energy 247 (2019) 155–170. https://doi.org/10.1016/j.apenergy.2019.04.020

[9] M. Zinzi, S. Agnoli, G. Ulpiani, B. Mattoni, On the potential of switching cool roofs to optimize the thermal response of residential buildings in the mediterranean region, Energy Build. 233 (2021) 110698. https://doi.org/10.1016/j.enbuild.2020.110698

[10] S. Shafiee, E. Topal, A long-term view of worldwide fossil fuel prices, Appl. Energy 87 (3) (2010) 988–1000. https://doi.org/10.1016/j.apenergy.2009.09.012

[11] S.R. Department, Durchschnittlicher Verbraucherpreis für leichtes Heizöl in Deutschland in den Jahren 1960 bis 2024, accessed on 2024-03-08. https://de.statista.com/statistik/daten/studie/2633/umfrage/entwicklung-des-verbraucherpreises-fuer-leichtes-heizoel-seit-1960/

[12] C. Arndt, X. Diao, P. Dorosh, K. Pauw, J. Thurlow, The ukraine war and rising commodity prices: implications for developing countries, Glob. Food Sec. 36 (2023) 100680. https://doi.org/10.1016/j.gfs.2023.100680

[13] J. Heider, N. Conrad, T. Stark, A. Abdulganiev, P. Kosack, A.-K. Wagner, Forschungsprojekt IR bau, HTWG Konstanz (2020). https://www.htwg-konstanz.de/fileadmin/pub/ou/energie/Forschung/IR-Bau/Abschlussbericht_Forschungsprojekt_IR-Bau.pdf

[14] P. Kosack, Beispielhafte vergleichsmessung zwischen infrarotstrahlungsheizung und gasheizung im altbaubereich, TU Kaiserslautern Arbeitkreis Ökologisches Bauen (2009). https://www-user.rhrk.uni-kl.de/~kosack/menu1/ForschungsberichtIR.pdf

[15] P. Kosack, Leitfaden infrarotheizungen, IG Infrarot Deutschland (accessed on 2024-05-15). https://ig-infrarot.de/leitfaden-infrarotheizung/

[16] I.G. Infrarot, Energetische Bewertung des Einsatzes von Infrarotheizungen als Spitzenlastabdeckung in Kombination mit einer Wärmepumpe für verschiedene Baualtersklassen, accessed on 2024-11-01. https://ig-infrarot.de/studie-tu-dresden-2024/

[17] T. Stark, J. Heider, N. Conrad, N. Bachmann, Forschungsprojekt IR bau 2, HTWG Konstanz (2024). https://www.htwg-konstanz.de/fileadmin/pub/ou/energie/Forschung/IR-Bau_2/Abschlussbericht_Forschungsprojekt_IR-Bau_2.pdf

[18] P.O. Fanger, Thermal Comfort: Analysis and Applications in Environmental Engineering, Thermal comfort: analysis and applications in environmental engineering, McGraw-Hill, New York, New York, 1972 - 1970.

[19] I.O.f. Standardization, Ergonomics of the thermal environment-Analytical determination and interpretation of thermal comfort using calculation of the PMV and PPD indices and local thermal comfort criteria, Technical Report ISO 7730:2005, ISO, 2005.

[20] AMEV, RLT-Anlagen, 2.1.1, accessed on 2024-12-12. https://www.amev-online.de/AMEVInhalt/Planen/Maschinenbau-und-Versorgungstechnik/RLT-Anlagen/RLT-Anlagen_Stand_01.07.2023.pdf

[21] K. Siebertz, D. van Bebber, T. Hochkirchen, Statistische Versuchsplanung: Design of Experiments (DoE), VDI-Buch, Springer Berlin Heidelberg, 2017.

[22] F. Tartarini, S. Schiavon, Pythermalcomfort: a python package for thermal comfort research, SoftwareX 12 (2020) 100578. https://doi.org/10.1016/j.softx.2020.100578

[23] Dantec, Signal Conversion, accessed on 2024-11-01. https://service.dantecdynamics.com/help/comfortsense/default.htm#Signal%20Conversion.htm

[24] L. Schmitt, M. Kriegel, Radiative heat transfer coefficients for surface heating and cooling systems in indoor spaces considering radiatively participating gases, Energy Build. 328 (2025) 115125. https://doi.org/10.1016/j.enbuild.2024.115125